

## 4. PARTICIPATION IN THE ASDEX UPGRADE PROGRAMME<sup>1</sup>

M.E. Manso (Head), F. Serra (Deputy Head), A. Combo, A. Ferreira, A. Silva, D. Borba, F. Salzedas, F. Silva, I. Nunes, J. Santos, L. Cupido, L. Fattorini, L. Guimarães, L. Meneses, P. Varela, R. Coelho, S. Hacquin, S. Graça, T. Ribeiro

### 4.1. INTRODUCTION

The Portuguese participation in the ASDEX Upgrade<sup>2</sup> (AUG) programme has been mainly focused in two research lines:

- Microwave reflectometry;
- MHD, turbulence and transport.

### 4.2. MICROWAVE REFLECTOMETRY

#### 4.2.1. Introduction

This research line included in 2005 activities on microwave systems and electronics, control and data acquisition, diagnostic developments, data processing, modelling and plasma physics studies.

Concerning *microwave systems and electronics*, the V band LFS channel was tested and electronics had to be modified for homodyne detection due to the degradation of the mixer. After its repair it was changed back again to heterodyne. The main control switch board of the system was calibrated and a faulty optical coupler was replaced. The pig-back of the optical analogue signal transmitters was changed. V band/X-mode channel was tested and changed from heterodyne to homodyne detection. All the diagnostic channels were inspected and tested. Part of the transmission line of the Q/X-mode channel was disassembled, tested and calibrated after high losses that were found to be caused by metal peaces of soldering material inside one of the waveguides. The V/X-mode antenna was modified to correct a construction error. A new transmission line for the HFS channels is being studied in order to protect the diagnostic in AUG forthcoming experiments with increased ECRH power.

Regarding *control and data acquisition*, the firmware of all of the eight control boards was upgraded to use a high level language, like the one used in the fluctuations monitor control system. This makes the communication more robust. Control software for a new “hopping” frequency system has being installed and tested. Also a new system has started to be developed.

Concerning *diagnostic developments*, the new hopping diagnostic was completed and first turbulence results were obtained.

Regarding *data processing*, a new algorithm was developed for the time-frequency analysis of broadband

signals which allows the length of the analysis window of the spectrogram to be adapted to automatically to the local time-frequency characteristics of the signals while maintaining a good time-frequency resolution. Several upgrades were also made to the interactive data analysis tools for better efficiency and less computing time.

Concerning *modelling*, dedicated tools were developed to simulate Doppler reflectometry. A code was developed for the analysis of turbulence and transport in the SOL.

The *plasma physics studies*: were focused mainly in pellet experiments as well as MHD, turbulence and transport. The studies could be extended to higher densities with the W band channel in full operation.

#### 4.2.2. Frequency calibration

The frequency calibration system was upgraded with a delay line. The output of the detected signal resulting from interference between the non delayed and the delayed signal as well as the spikes from the frequency markers are shown in Figure 4.1. The interference data was used to obtain a continuous the frequency versus time characteristics of the oscillators in ultrafast swept operation.

The instantaneous phase evolution of the signal shown in Figure 4.1a is obtained with an Hilbert Transform and the resulting frequency step is depicted in Figure 4.1b. The spectrogram of a signal reflected from a metallic mirror obtained with the frequency marker calibration shows significant deviations from a constant value corresponding to the distance between the antenna and the mirror (Figure 4.2a), whereas in the case of the delay line calibration an almost constant time delay is recovered (Figure 4.2b). The novel method greatly improved the accuracy of density profiles.

#### 4.2.3. Control and data acquisition

In order to exploit full diagnostic capabilities of the ASDEX Upgrade tokamak it is mandatory to upgrade the data acquisition and control system. This will cope with faster frequency sweep times and improved time resolution as well as accuracy allowing, for example, plasma position and shape measurements for control purposes, as it is foreseen for ITER. A new PCI-based

<sup>1</sup> Work carried out in collaboration with the ASDEX-Upgrade Team. Contact Person: Dr. G. Conway.

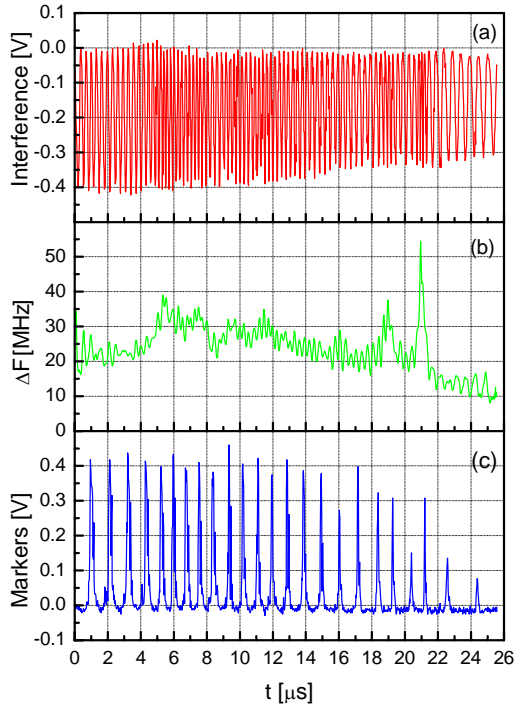


Figure 4.1 - a) Interference signal. b) Frequency step from the interference signal. c) Frequency markers signal.

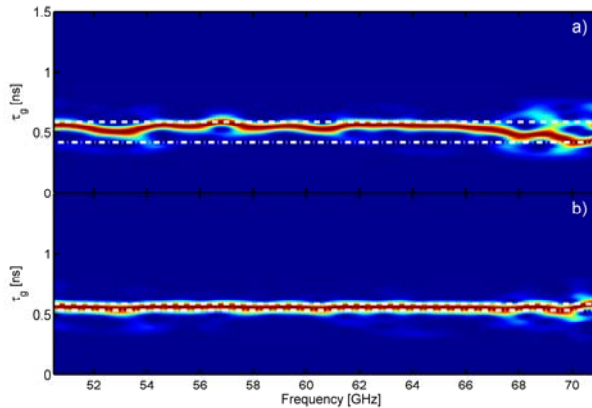


Figure 4.2– Spectrogram of a signal reflected from a metallic mirror: a) frequency marker calibration and b) delay line calibration.

system (Figure 4.3) is being developed based on a digitizer card with 2 channels, 12-bit resolution and a waveform generator with one channel, 14-bit resolution. Both cards will have 512 Mbytes of memory, a Digital Signal Processor (DSP) for advanced processing modes and a Field Programmable Gate Array (FPGA) for real-time algorithms and complex trigger managing modes. The system will be able to support multiple cards (digitisers and signal generators) operating synchronously at a maximum

speed of 210 MHz. The development of the fast digitizers and generators was started with the schematic and layout design of the PCI cards.

#### 4.2.4. Numerical studies for plasma position

The sensitivity and robustness of reflectometry to track plasma movements in a steady state ELMy H-mode scenario was studied aiming to fully demonstrate the use of reflectometry for control purposes as foreseen for ITER. Position curves after ELM removal were averaged using a window of 3 measurements or 26 ms, roughly equivalent to averaging three ITER individual measurements (at a 10 ms rate). To compensate the errors in the profile inversion due to the non probed plasma region with O-mode reflectometry, a dynamic initialization procedure was developed.

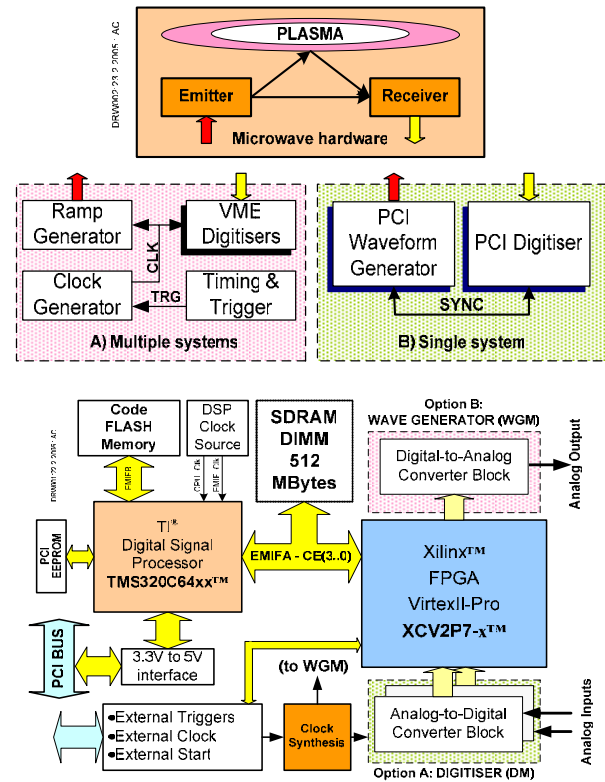


Figure 4.3 - Current (A), new (B) data acquisition system and PCI module diagram.

To track the separatrix position from reflectometry profiles two estimations for the density at the separatrix were used one from diagnostic XPTO and multiplying the average density by a factor  $\alpha$  (with  $\alpha \in [0.15, 0.65]$ ). Position results obtained using the dynamic estimation for the ratio between the separatrix density and the average density after removing measurements performed during ELMs, were impressively good (Figure 4.4). In this case, shot #19701, the tracking of the separatrix position using

a fixed scaling of 30% of the average density to estimate the density at the separatrix would result in a match to the magnetic separatrix with a radial error of 2.5 mm and standard deviation of 2.5 mm both at HFS and LFS.

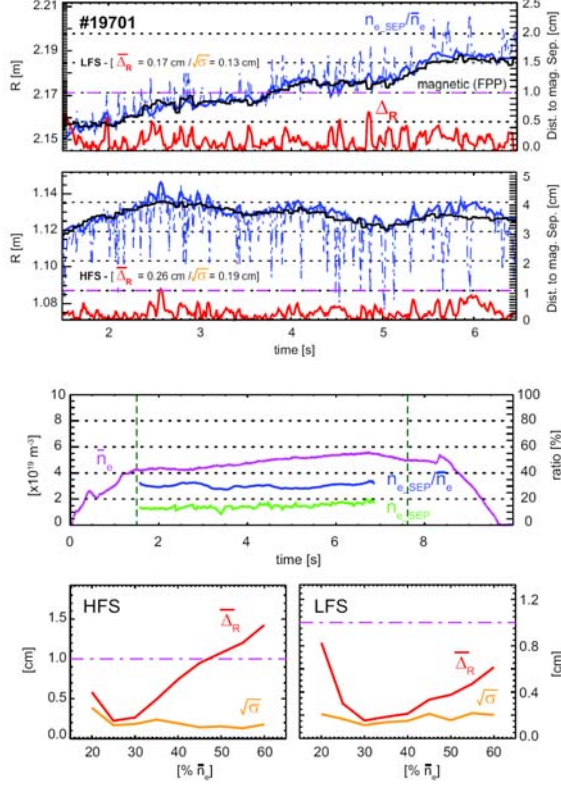


Figure 4.4 - Position of density layers corresponding to  $n_{e\_sep} / \bar{n}_e$  after removing during-ELM measurements and averaging during a 26 ms window (thick blue) and the corresponding distance to the magnetic separatrix,  $\bar{\Delta}_R$  (red), in discharge #19701;  $\bar{n}_e, n_{e\_sep}$  and corresponding ratio curve (top right plots);  $\bar{\Delta}_R$  and  $\sqrt{\sigma}$  as a function of a static percentage of  $\bar{n}_e$  (bottom right plots).

#### 4.2.5. Modelling<sup>2</sup>

The previously developed 2D code is being equipped with the tools to explore the possibilities of extracting information from reflectometry about thin velocity shear layers as those occurring, for example, in internal transport barriers and zonal flows.

The numerical results can be applied to any reflectometry system, namely in ASDEX Upgrade or Tore Supra<sup>3</sup>.

<sup>2</sup> Work carried out in collaboration with Dr. Stephan Heuraux (Université Poincaré, Nancy, France.)

<sup>3</sup> Modelling analysis more focused on reflectometry for ITER is presented in section 8.

The plasma is modelled with a generic density profile, across circular or elliptical iso-density lines (slab model corresponds to an infinitely elongated ellipsis). Turbulence is taken into account as a sum of modes with random phase. The density perturbation at each point obeys to,

$$\delta n_{eTRB} = \sum_{i_m} \sum_{j_m} A(i, j) \cos[k_x(i)x + k_y(j)y + \varphi(i, j)] \quad (1)$$

The choice of the coefficients  $A(i, j)$  is in agreement with the Tore Supra experimental data. The columns of the original turbulence matrix on the shear region are shifted poloidally, each column sliding at a speed given by the imposed velocity shear profile. Figure 4.5 shows the columns of the original turbulence matrix  $n_e(r, t)$  (top left), as the simulation runs its course, slide with a velocity given by the shear profile. Its effect on the turbulence structure is shown on Figure 4.5 (bottom left). This model for velocity shear implies a modification of the wavenumber spectrum (k-spectrum) on the shear layer (both poloidal and radially). Figure 4.5 shows the original spectrum (top right) and the spectrum at iteration  $50 \times 10^3$  (bottom left) are shown. They reveal the deformation of the density fluctuation spectrum in the shear zone reflecting the elongation of the turbulent structures along the poloidal direction and the radial squeezing as the matrix columns slide in the shear region.

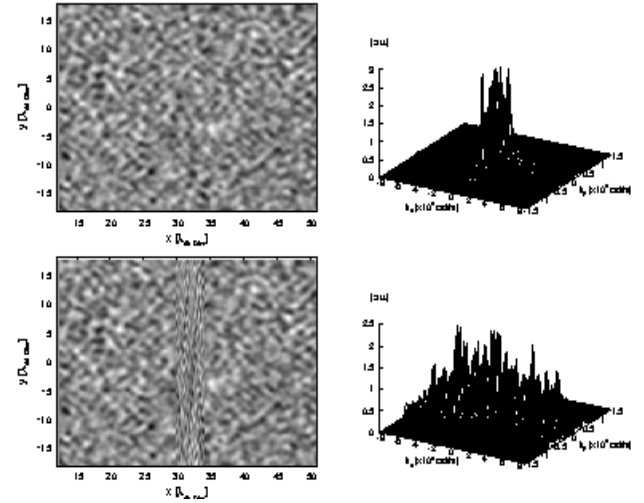


Figure 4.5 - Original turbulence matrix (top left) and the amplitude k-spectrum (top right). Matrix of turbulence at iteration  $50 \cdot 10^3$  (bottom left) and the modified spectrum at the poloidal velocity shear region with a radial profile in the x-direction (bottom right).

In classical reflectometry the code is usually run in a monostatic setup (same antenna used for emission and reception) and the signal is excited in the waveguide using a Unidirectional Transparent Source (UTS) allowing

unidirectional injection of a wave. Figure 4.6 (upper plot) presents a monostatic setup for a 2D H-plane horn with a half power beam width of  $30^\circ$  appears on top. The Doppler effects in this configuration appears due to lateral probing of the plasma through the relatively large antenna radiation pattern. The contribution to the frequency spectrum from the direct reflection on the plasma is stronger than the Doppler effects and the Doppler frequency shift arises on a wide frequency range according to the Bragg law at the turning point (oblique cut-off).

The 2D code was adapted to typical Doppler reflectometry using an optical system (Figure 4.6 bottom plot). The use of a lens allows the emission of a quasi non-diverging beam with a planar wave front which will respond to a single wave number according to the injection angle chosen by the prism. The same impulsive response (IR) technique utilized to implement the UTS is used to eliminate the spurious reflection from the lens and prism.

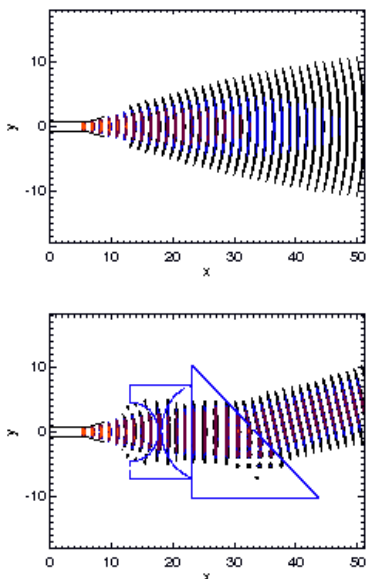


Figure 4.6 Classical reflectometry with a horn (top) and Doppler setup with a converging lens and prism to launch beams with high directivity.

#### 4.2.6. Pedestal evolution in the presence of ELMs

The study of the pedestal evolution in AUG discharge #1991, where four intrinsic type I ELMs and one pellet triggered ELM occurred, is presented in Figure 4.7, along with the time traces of the line average density obtained with the interferometer diagnostic, and the  $H_\alpha$  radiation associated with the outward particles flux into the divertor plates.

A further picture of edge profile dynamics under ELMs was obtained from the detailed profile evolution at the LFS (Figure 4.8). At the LFS the density time traces show clearly the two distinct regions separated by  $\sim 1$ cm around 2.17 m. This should be the position of the last closed flux surface, separating the pedestal ( $< 2.17$  m) and the scrape of

layer (SOL) ( $> 2.17$  m). Transport during the ELM (period of enhanced  $D_\alpha$  light emission) increases the SOL density during that period of time.

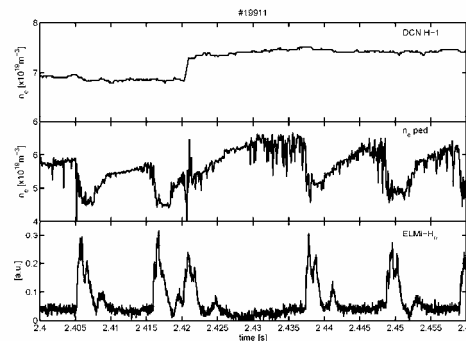


Figure 4.7 – Time traces of: (a) line average density from interferometry (DCN H-1); (b) pedestal height from reflectometry (ne-ped); (c)  $H_\alpha$  radiation (ELM- $H_\alpha$ ).

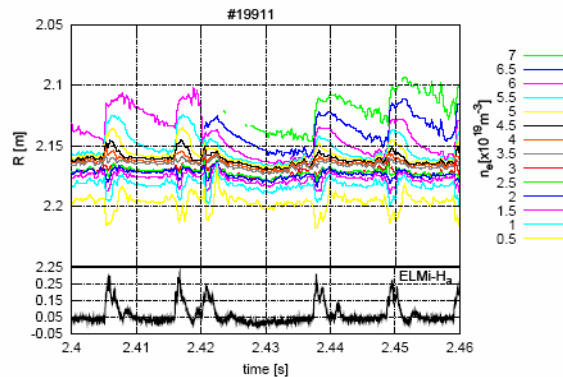


Figure 4.8 – Density contour plots showing the time evolution of the edge density profile at the LFS. The bottom plot depicts the time trace of  $H_\alpha$  radiation (ELM- $H_\alpha$ ).

The high SOL density is maintained during the ELM, but is back to pre-ELMs values immediately after the end of the period of enhanced  $D_\alpha$  light emission. This corresponds to a low confinement expected for the SOL and the higher density can only be maintained by the strong influx of particles to the SOL from the core during the ELM. The density in the pedestal also collapses very quickly, within 100  $\mu\text{s}$  time scale, but recovers more slowly to the pre-ELM values taking  $\sim 10$ -20 ms, which is approximately the ELM repetition time. This means that the confinement in the pedestal is good between ELMs, allowing the profiles to recover, but poor during the ELMs. This is consistent with the expected picture of the density evolution in the pedestal and SOL regions during the ELM cycle.

#### 4.2.7. Localization of TAE modes

The new hopping reflectometer has the capability of probing several density cutoff layers (in the Q and V

bands at LFS) during each discharge. The position of density layers is determined using  $n_e$  profiles from the broadband FM-CW reflectometry system.

First results (Figure 4.9) show that in TAE experiments (AUG shot #20489), with low density ( $\bar{n}_e = 3.25 \times 10^{19} m^{-3}$ ), 5 MW of ICRH power and L-mode, the “hopping frequency system” allows the radial localization of modes at the edge as well as TAEs and sawteeth precursor in the core ( $\rho_{pol} = 0.6-0.35$ ) clearly separated from the edge. These results are important to study the radial structure of TAEs modes.

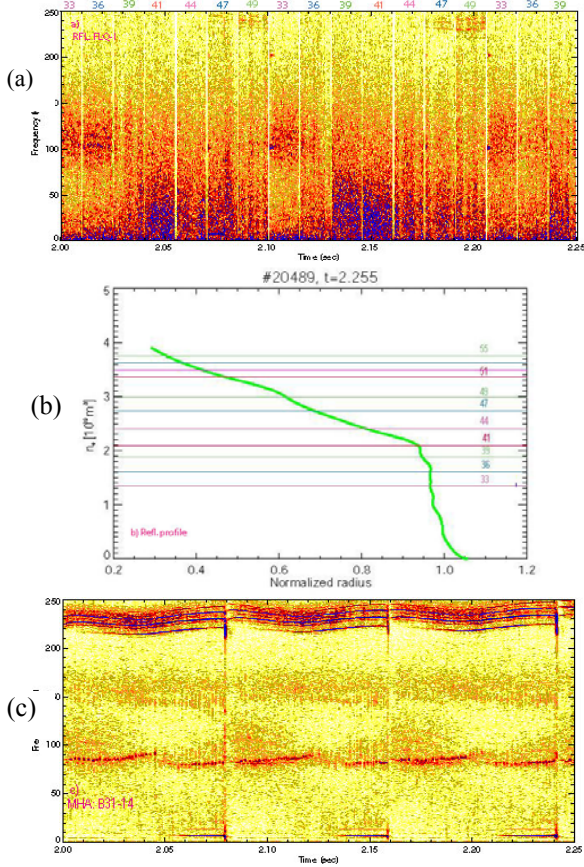


Figure 4.9 - Spectrogram of Q band “hopping frequency millimeter wave reflectometer” for TAE shot #20489 (a), the corresponding density profile from reflectometry for the localization of the density cutoff layers (b) and spectrogram from magnetics (c).

### 4.3. STUDIES ON MHD, TURBULENCE AND TRANSPORT

#### 4.3.1. Introduction

This research line included in 2005 code development for turbulence and transport analysis in the SOL of ASDEX-Upgrade.

#### 4.3.2. Code development for turbulence and transport analysis in the SOL of ASDEX Upgrade

The boundary of tokamak plasmas is characterised by electromagnetic interactions between wavelike and fluidlike motions on space scales down to the ion gyroradius. The two moment gyrofluid flux tube model GEM3 was used to investigate electromagnetic turbulence and the associated transport phenomena both in the edge and scrape-off layer (SOL) of such region of the plasma. The comparative study between edge and SOL conditions was concluded. The main results include the observation of the dominance of a convective cell mode ( $k_{\perp} \neq 0$  and  $k_{\parallel} = 0$ ) whenever the limiter was included, i.e., whenever the SOL boundary conditions were applied, in accordance with the experimental observations for the SOL region. The turbulent transport values were also found to increase in the latter situation, where the large scale interchange dynamics became dominant, due to the absence of the adiabatic response of the electrons in the convective cell mode. Conversely, with closed field lines boundary conditions, the field line connection of tokamak sheared magnetic fields suppresses the convective cell mode, when the flux surfaces are closed, leaving the drift wave character typical of the plasma edge, with the parallel electron dynamics keeping the electrostatic potential coupled to the electron pressure through parallel forces mediated by parallel currents.

The study of the effect of the equilibrium magnetic field geometry of a tokamak (ASDEX Upgrade with diverted geometry) was continued, including the investigation of the issue of the spatial resolution of the simulations. This also included verifications made within the geometry code METRICS to check the consistency of the coordinates transformations made, and also the implementation of a Savitzky-Golay smoothing filter, constituting an improvement of the filtering that is necessary to apply to the curvature operators in the case of grids coming from the CARRE code.

The results for closed flux surfaces regions showed a well spatially resolved system, even at the locations along the field lines where the grid cells are most severely deformed, due to the variations of the perpendicular (contravariant) metric components of the metric (Figure 4.10). When compared to the corresponding results obtained with the simplified geometry model (Figure 4.11), which retained only the poloidal dependence of the curvature operators, they revealed a reduction of the measured  $E \times B$  turbulent transport, which brought the figures closer to experimentally measured values. This result supports the scenario whereby the local magnetic shear, that affects directly the polarisation dynamics (the main mechanism behind a fluid drift model) and is particularly strong close to the magnetic separatrix (Figure 4.11–left), facilitates the nonlinear decorrelation processes by twisting the turbulent perpendicular vortical structures, which are then torn apart to smaller scales.

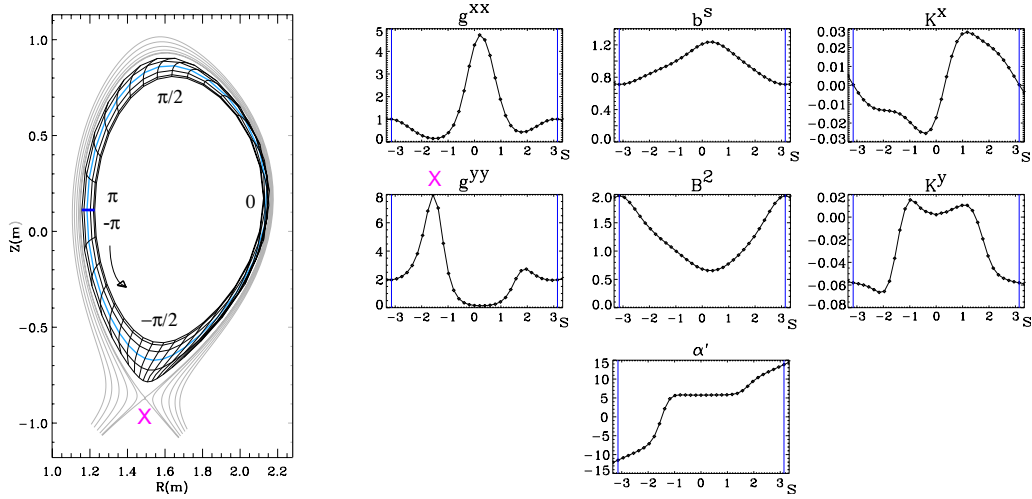


Figure 4.10 - (left) Representation of the ASDEX Upgrade diverted equilibrium magnetic field used herein; (right) 7 geometrical quantities necessary describing the equilibrium on the left side figure, which are needed to be provided to GEM or GEM3 models. The curves were calculated for the flux surface highlighted in blue on the left side figure.

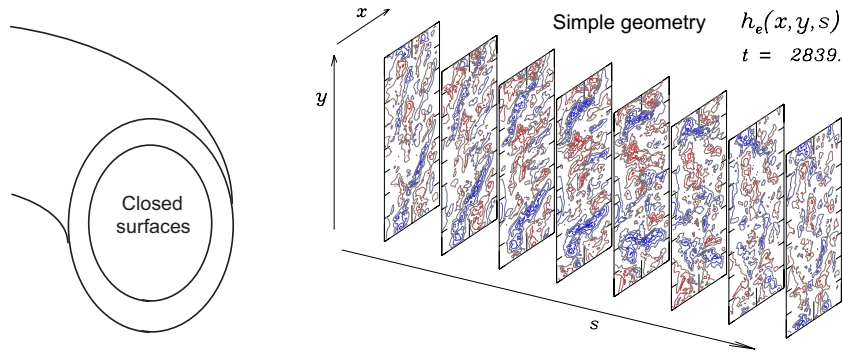


Figure 4.11 - 3D spatial morphology of the nonadiabatic electron density “ $h_e = ne - \phi$ ” ( $n_e$  is the electron density and  $\phi$  is the electrostatic potential) in the computational domain for closed flux surfaces (edge), using the simplified model for the tokamak geometry. Negative values are represented in blue and positive in red.

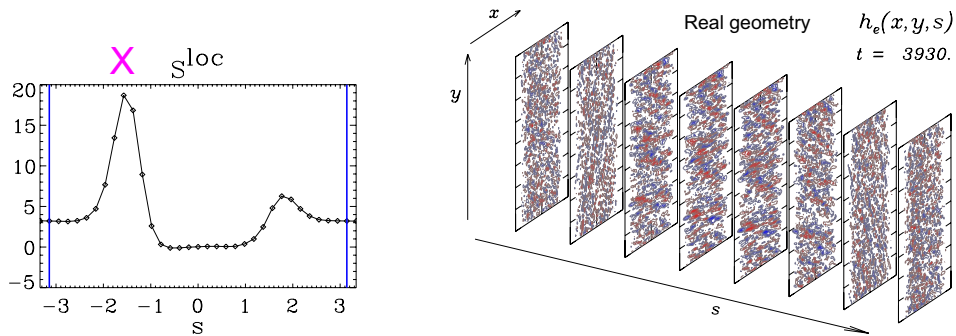


Figure 4.12 - (left) Local shear along a magnetic field line, a quantity which is absent in the simplified geometry model used for figure 2; (right) The same as in figure 2, but using the realistic description of the tokamak (figure 4.10). Note the relation between the maxima of the local shear and the twisting of the vortical structures in the plane perpendicular to the magnetic field. Compare with figure 2, where bigger perpendicular structures are present.